

# Low-Temperature Photoluminescence Investigation of Light-Induced Degradation in Boron-Doped CZ Silicon

Katharina Peh,\* Kevin Lauer, Aaron Flötotto, Dirk Schulze, and Stefan Krischok

Light-induced degradation (LID) in boron-doped Czochralski grown (CZ) silicon is a severe problem for silicon devices such as solar cells or radiation detectors. Herein, boron-doped CZ silicon is investigated by low-temperature photoluminescence (LTPL) spectroscopy. An LID-related photoluminescence peak is already found while analyzing indium-doped *p*-type silicon samples and is associated with the  $A_{Si}-Si_i$  defect model. Herein, it is investigated whether a similar peak is present in the spectra of boron-doped *p*-type CZ silicon samples. The presence of change in the photoluminescence signal intensity due to activation of the boron defect is investigated as well. Numerous measurements on boron-doped samples are made. For this purpose, samples with four different boron doping concentrations are analyzed. The treatments for activation of the boron defect are based on the LID cycle. During an LID cycle, an additional peak or shoulder neither in the areas of the boron-bound exciton transverse acoustic and nonphonon-assisted peaks ( $B_{TA}$ ,  $B_{NP}$ ) nor in the area of the boron-bound exciton transverse optical phonon-assisted peak ( $B_{TO}$ ) is found. The defect formation also does not lead to a lower photoluminescence (PL) intensity ratio  $B_{TO}(BE)/I_{TO}(FE)$ .

## 1. Introduction

Light-induced degradation (LID)<sup>[1,2]</sup> in *p*-type silicon (e.g., doped by boron or indium) is still attributed to an unknown defect. This kind of defect was reviewed in other studies.<sup>[3,4]</sup> The dopant is one of the participating factors in the formation of this defect. Currently, the demand for silicon for photovoltaic cells and radiation detectors is very high. Therefore, improving the devices

efficiency is of utmost importance. That is why LID just came back into the spotlight for research. The defect occurs mainly in single-crystal CZ-grown silicon which is why we are choosing CZ Si for our studies. An interesting observation is the dependence of the LID defect density on the oxygen concentration.<sup>[5]</sup> Therefore, the involvement of oxygen in the defect (boron oxygen defect) is often assumed. For this reason, the boron oxygen LID defect has been proposed.<sup>[6]</sup> Instead of the boron oxygen defect we propose the formation of  $A_{Si}-Si_i$  defect (A: substitutional acceptor, i: interstitial silicon) to explain LID.<sup>[7]</sup> This does not involve oxygen in the defect. However, defect formation is catalyzed by oxygen clusters.

In our work, we mainly want to investigate the LID defect using low-temperature photoluminescence (LTPL). Previous studies on silicon impurified with indium, boron, and iron served as the basis for our research. They showed how a defect


can affect the photoluminescence spectrum. During these external and internal works, which include illumination and/or annealing of the samples, the following was observed.

An LID-related PL peak called P line could be detected in indium-doped samples by LTPL.<sup>[8]</sup> Another study showed the formation of a shoulder of the transversal optical boron-bound exciton ( $B_{TO}(BE)$ ).<sup>[9]</sup> Also, a reduction of the  $B_{TO}(BE)/I_{TO}(FE)$  ratio was observed due to the formation of iron–boron pairs.<sup>[10]</sup>  $I_{TO}(FE)$  denotes the intrinsic luminescence peak caused by the transverse optical phonon-assisted recombination of free excitons. Here, iron–boron complexes were observed after thermal annealing. The pairing reaction leads to a reduction of the  $B_{TO}(BE)/I_{TO}(FE)$  ratio.

In charge carrier lifetime measurements, the so-called LID cycle is visible in samples doped with indium and boron.<sup>[5,11]</sup> In gallium-doped samples, the LID cannot be detected by lifetime measurement. The LID cycle is composed of recurring sample treatments. These include illumination and annealing steps based on charge carrier lifetime measurements. See Möller et al.<sup>[11]</sup> and Bothe et al.<sup>[5]</sup> The charge carrier lifetime decreases in two steps during illumination and increases to the initial value with one annealing (200 °C for 10 min) step. The aim of this work is to study the possible photoluminescence features of the  $B_{Si}-Si_i$  defect in boron-doped samples. This contribution also intends to outline the LTPL parameters needed for accurate measurements of the  $B_{TO}(BE)/I_{TO}(FE)$  ratio and their impact on the PL spectra.

K. Peh, K. Lauer, A. Flötotto, D. Schulze, S. Krischok  
 Institut für Physik und Institut für Mikro- und Nanotechnologien  
 TU Ilmenau  
 98693 Ilmenau, Germany  
 E-mail: katharina.peh@tu-ilmenau.de

K. Lauer  
 CiS Forschungsinstitut für Mikrosensorik GmbH  
 Konrad-Zuse-Str. 14, 99099 Erfurt, Germany

 The ORCID identification number(s) for the author(s) of this article can be found under <https://doi.org/10.1002/pssa.202200180>.

© 2022 The Authors. physica status solidi (a) applications and materials science published by Wiley-VCH GmbH. This is an open access article under the terms of the Creative Commons Attribution-NonCommercial License, which permits use, distribution and reproduction in any medium, provided the original work is properly cited and is not used for commercial purposes.

DOI: 10.1002/pssa.202200180

The investigation of the LID was primarily done by LTPL measurements but also by microwave-detected photoconductance decay (MWPCD).

This article is meant to present our experimental results. It compares the predetermined hypothesis (or theory) with the actual measured values. Furthermore, it compares and interprets the measurement results with those of other teams. For this purpose, we adopt already published evaluation methods for sample temperature determination. These evaluation methods are briefly discussed and compared.

## 2. Experimental Section

### 2.1. Samples and Treatment

The experimental setup consisted of five different samples of different impurity concentrations  $c_i$  ( $c$  = concentration,  $i$  = dopant symbol). Four CZ-Si wafers with different boron doping between  $c_B = 1.2$  and  $8.7 \times 10^{15} \text{ atoms cm}^{-3}$  were used to study the boron-induced  $B_{Si}-Si_i$  defect. In addition, a reference sample (float-zone Si) was analyzed. This sample was only slightly doped with phosphorus ( $c_p = 4.4 \times 10^{11} \text{ atoms cm}^{-3}$ ).  $1 \text{ cm} \times 1 \text{ cm}$  samples were cleaved from the wafers. The sample parameters determined among others by four-point-probe measurements are listed in Table 1.

#### 2.1.1. Sample Treatment for Low-Temperature Photoluminescence Measurements

In our study, great emphasis is placed on the detailed description of the sample treatment and its procedure. Based on our studies of the  $In_{Si}-Si_i$  defect, we assumed that the defect exists in different configurations.<sup>[11]</sup> It is important in which configuration the defect is at the time of further treatment. For this reason, the measurement routine and sample treatment were done as follows: sample treatment, LTPL measurement, sample treatment, LTPL measurement, and so on.

The measurement results with their corresponding treatments are presented here: samples illuminated for 60 h at  $40^\circ\text{C}$  and one sun intensity abbreviated by (I), samples illuminated for 1 h at  $40^\circ\text{C}$  and one sun abbreviated by (i), and samples

annealed for 10 min at  $200^\circ\text{C}$  in the dark abbreviated by (t) but also, some samples, measured after 24 h at  $40^\circ\text{C}$  and one sun treatment.

A commercial 500 W halogen radiator with a radiation power of  $1 \text{ sun}$  ( $1000 \text{ W m}^{-2}$ ) was used to illuminate the samples. During illumination, the sample temperature was kept constant at  $40^\circ\text{C}$ . For annealing in the dark, a temperature-controlled hot plate under ambient atmosphere was used.

#### 2.1.2. Sample Treatment for MWPCD Measurements

For the lifetime measurement, the sample  $c_B = 8.7 \times 10^{15} \text{ cm}^{-3}$  was annealed for 10 min at  $200^\circ\text{C}$  in the dark before the illumination.

### 2.2. Low-Temperature Photoluminescence Measurements

The LTPL apparatus was constructed as follows. It consisted of a frequency-doubled Nd:YAG laser (532 nm). The sample chamber was enclosed by a helium (He) flow cryostat.

The helium flow cryostat was surrounded by a liquid nitrogen reservoir that reduced thermal radiation losses. The cryostat was precooled to 77 K and was again surrounded by a UHV chamber for insulation. A collecting lens focused the emitted radiation on the entrance slit of an imaging monochromator with a focal length of  $2 \times 750 \text{ mm}$  and exchangeable line grids with 1200 and 150 grooves  $\text{mm}^{-1}$ , respectively. The spectra were measured by InGaAs single-line detector. PL spectra were recorded with excitation powers of 100, 500, and 1000 mW and beam diameter of about 2 mm. This measurement cycle was identical for all measurements. The laser light was directed onto the samples through prisms and windows with a loss of about 50%. All measurements were integrated to  $5 \times 10 \text{ s}$ . A vaporizer with a wound heater (maintained at around 20 % heating power) was used to set the sample temperature to  $T = 10 \text{ K}$ , which was controlled by a sensor attached slightly below the sample. Both the sample and the sensor were attached with screws to a copper sample holder, which was located in the He gas flow. The sensor temperature was used to label the figures. The sample holder consisted of six sample positions which together comprised one run.

The nomenclature of PL spectra and ratios was made according to SEMI MF1389 regulation,<sup>[12]</sup> following Dean et al.<sup>[13]</sup> and Tajima et al.<sup>[14]</sup>

### 2.3. Four-Point-Probe Measurements

To validate the dopant concentration specified by the manufacturer, we made four-point-probe measurements (see Table 1). The mean values of the results of the four-point-probe measurements at room temperature were used for sample labeling in all graphs in this article. The layer resistance measurement device of the company Jandel scientific was used.

### 2.4. MWPCD Measurements

The MWPCD method was used to check the presence of the LID defect in the samples.<sup>[15]</sup> It is used to determine the carrier lifetime. The inverse carrier lifetime is proportional to the LID

**Table 1.** a) Four-point-probe measurement on boron-doped silicon samples, all samples were measured six times at the center and six times at the edge, and the mean value was taken from them. The error was the standard deviation of the 12 measurements. b) Wafer parameters according to manufacturer.

Measurement resistance [ $\Omega\text{cm}$ ]	Wafer thickness [ $\mu\text{m}$ ]	Calculated doping [ $\text{cm}^{-3}$ ] (mean value)
<b>a</b>		
		boron
$11.14 \pm 0.16$	525	$1.22 \times 10^{15}$
$8.43 \pm 0.03$	525	$1.63 \times 10^{15}$
$2.36 \pm 0.02$	525	$6.06 \times 10^{15}$
$1.68 \pm 0.01$	475	$8.67 \times 10^{15}$
<b>b</b>		
		phosphorus
10 000	525	$4.41 \times 10^{11}$

defect density. The carrier lifetime was measured at an excess carrier density of  $\Delta n = 5 \times 10^{14} \text{ cm}^{-3}$ . The MWPCD excitation laser with an average intensity of  $I = 10 \text{ mW cm}^{-2}$  was used to illuminate the samples. A temperature of  $T = 40^\circ \text{C}$  was held during both the lifetime measurement and the sample illumination.

## 2.5. Sample Temperature Determination Using a Curve Fit

An essential part of this work was the evaluation of PL spectra. Due to the temperature dependence of PL spectra, the sample temperature can be used to draw conclusions about the measurement stability. The excitation power influences the sample temperature and thus the detected PL spectrum. Therefore, a suitable method for the determination of the sample temperature has to be applied. We found this in Pelant et al.<sup>[16]</sup> This is because stable measurement conditions and evaluation methods are of crucial importance, especially for the question of whether activation of the  $\text{B}_{\text{Si}}\text{-Si}_i$  defect leads to a reduction in the  $\text{B}_{\text{TO}}(\text{BE})/\text{I}_{\text{TO}}(\text{FE})$  intensity ratio.<sup>[10]</sup>

The line shape of the free exciton emission of Si ( $I_{\text{FE}}(h\nu)$ ) can be described by a Maxwell–Boltzmann distribution.<sup>[16]</sup>

$$I_{\text{FE}}(h\nu) \approx \sqrt{\frac{\hbar\nu}{k_B T}} e^{-\frac{\hbar\nu}{k_B T}} \quad (1)$$

with the parameters:  $\hbar\nu = h\nu - E_0$  (kinetic energy of exciton translation motion,  $E_0$  [low-energy cutoff of the FE emission line]) and  $k_B T$  ( $k_B$  temperature Boltzmann factor and  $T$  the temperature)

The half width ( $\delta$ ) of the FE peak linearly increases with temperature<sup>[16]</sup>

$$\delta \approx 1,8 k_B T \quad (2)$$

The sample temperature and the  $\text{B}_{\text{TO}}(\text{BE})$  peak height were determined according to Pelant et al.<sup>[16]</sup> in this work. **Figure 1** is presented to give a short overview of our spectra evaluation method. Figure 1a shows the fit curves of individual peaks

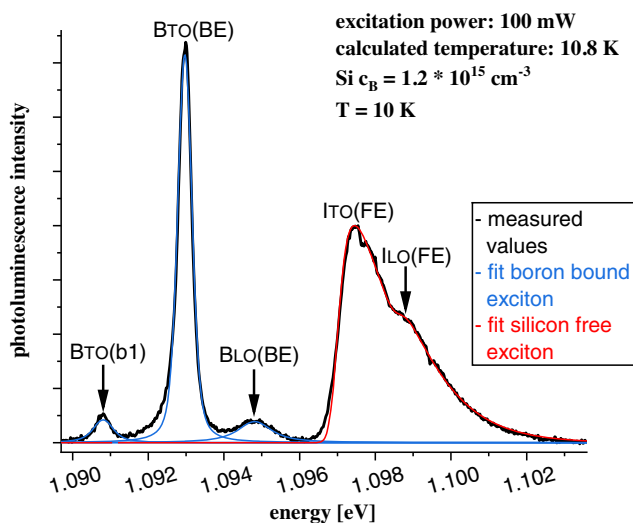


**Figure 1.** Applied curve fit of the free (FE) and bound (BE) excitonic transitions.

compared with the line shape of a photoluminescence spectrum of boron-doped silicon. The line shape of free exciton peaks is described by a Maxwell–Boltzmann distribution (see Equation (1)). The line shape of bound exciton peaks is described by a Lorentzian function. In order to consider slit broadening and broadening due to phonon collisions these functions have to be convolved with a Gaussian function. Therefore, during the fitting procedure, each peak in the spectrum was described separately by either a Maxwell–Boltzmann distribution or a Lorentzian function. The sum of these functions was convolved with a Gaussian function and then fit to the experimental spectrum. The sample temperature, which is explicitly part of the Maxwell–Boltzmann distribution, was one of parameters which were optimized during the fit.

## 3. Results and Discussion

The results section shows the presence of LID through the lifetime measurement in the first section. Then, we briefly discuss the peak fitting method and show differences in the analysis techniques in the second section. Furthermore, we evaluate our PL spectra with the help of these analysis methods. A comparison is made with the assumptions that the PL spectrum shows an additional radiating line (peak or shoulder) or that the  $\text{B}_{\text{TO}}/\text{I}_{\text{TO}}$  ratio is influenced by the LID.

### 3.1. Experimental Results of the Carrier Lifetime Measurement

With the charge carrier lifetime measurement, we verify the presence of the LID in our samples. **Figure 2** shows the result of the charge carrier lifetime measurement by MWPCD on the  $\text{Si } c_B = 8.7 \times 10^{15} \text{ cm}^{-3}$  samples. Here the inverse carrier lifetime is shown as a function of illumination time. The LID

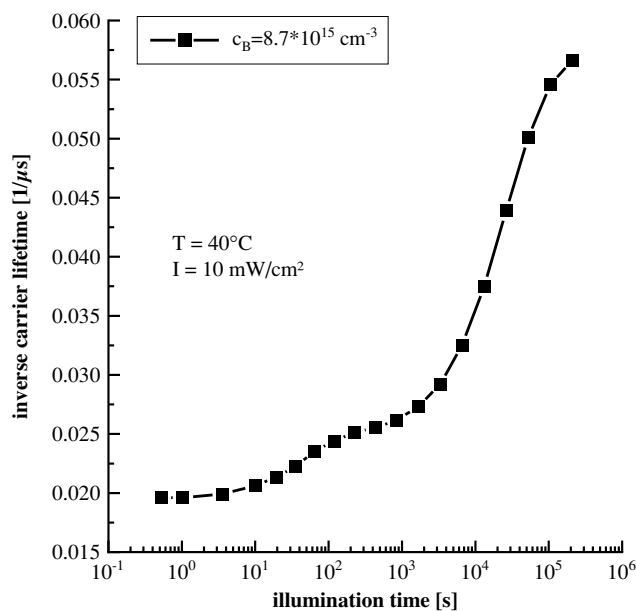


**Figure 2.** Inverse charge carrier lifetime as a function of illumination time for boron-doped CZ silicon. The LID can be observed here using MWPCD.

cycle contains a fast degradation and a slow degradation component. The degradation originates from a fast-forming recombination center (FRC) and a slow-forming recombination center (SRC). These recombination centers are called LID defects. This behavior can be confirmed by measurements of the charge carrier lifetime. The charge carrier lifetime is the average time interval that an excess charge carrier spends in the valence or conduction band before electron–hole recombination occurs. The activated defects are additional recombination centers and thus lead to the reduction of carrier lifetime. Up to about 4 min of illumination, the charge carrier lifetime is reduced from about 50 to 40  $\mu$ s. From approx. 4 to 16 min, the lifetime remains almost constant. From 16 min illumination to approx. 30 h, the lifetime slowly decreases to around 18  $\mu$ s. This behavior agrees with our expectations. It can be concluded that illumination has caused the formation of LID defects in the examined sample. A study by Möller et al.<sup>[11]</sup> was able to show that a two-step charge carrier lifetime degradation analogous to boron-doped silicon also occurs for indium under illumination. In addition, indium-doped silicon shows a P line in the photoluminescence spectrum (using LTPL). The P line intensity can be influenced similar to the charge carrier lifetime by illumination and annealing.<sup>[8]</sup> This leads us to believe that an additional photoluminescence line also occurs in boron-doped silicon.

### 3.2. Determination of the Sample Temperature

In the next step, we get to the detailed studies of the boron-doped samples using LTPL. Suitable evaluation methods are necessary for the understanding of PL spectra. **Figure 3** shows the comparison between the measured temperature at the sensor and the determined sample temperature. The transversal optical ( $I_{TO}(\text{FE})$ ) and the longitudinal optical ( $I_{LO}(\text{FE})$ ) FE lines of sample Si  $c_p = 4.4 \times 10^{11} \text{ cm}^{-3}$  were analyzed. The black squares show the temperature determined by the full width at half maximum of the  $I_{TO} + I_{LO}(\text{FE})$  double peak (see Equation (2)). The temperature values of the red squares were determined

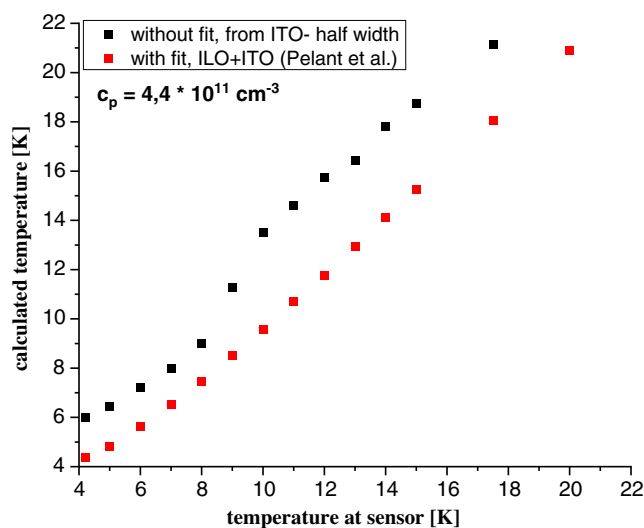


**Figure 3.** Calculated temperatures as a function of the temperature at the sensor.

by fitting the intrinsic PL peaks according to the method described in Section 2.5. Both temperature determination methods have been used in previous works.<sup>[16–18]</sup> In theory, both temperature determination methods should yield the same results. In all cases of temperature determination via the full width at half maximum, the calculated temperatures are higher than the temperatures measured by the sensor. The black squares increase linearly up to 8 K (sensor temperature). Then they show a step and increase linearly again from 10 K. Up to 8 K (sensor temperature), the calculated temperatures are about 1 K greater than the temperature read at the sensor. From 10 K, the temperature difference is around 3 K. The fit of the FE double-peak red squares yields a steady linear increase in sample temperature. The values coincide within an error of  $\Delta T \pm 0.5 \text{ K}$  to the sensor temperature. The origin of the step in the black squares is based on the FE double-peak structure. Up to 8 K (sensor temperature), the full width at half maximum is mainly determined by the  $I_{TO}$  peak. If the temperature rises, the  $I_{TO}$  and  $I_{LO}$  peaks increasingly overlap. In this article, we use the evaluation method according to Pelant et al.<sup>[16]</sup> (red squares in Figure 3) to determine the temperature of the samples. Here, the evaluation method shows a linear behavior at all temperatures. The temperature at the sensor and the calculated temperature also do not deviate that much from each other. Iwai et al.<sup>[17]</sup> published a method to determine B and P concentrations with LTPL using the full width at half maximum of the free exciton. See Equation (2). However, when the theoretical free exciton peak is considered, both the Gaussian broadening and the overlap of the  $I_{LO} + I_{TO}$  peaks at temperatures above 4.2 K must be taken into account. It remains to be mentioned that a calibration curve, for example, for the determination of the dopant concentration, can also be created with the help of the full width at half maximum of the FE peak. Here only strict limits have to be given (e.g.,  $T \geq 11 \text{ K}$ ). A reference measurement, for example, a four-point-probe measurement, must be made. This strict limit is based on the two straight lines of the black square in Figure 3. The step in between is based on the double-peak structure  $I_{LO} + I_{TO}$ . At a dopant concentration of  $4.4 \times 10^{11} \text{ cm}^{-3}$  between 8 and 10 K, the  $I_{LO}$  peak intensity is still below the  $I_{LO} + I_{TO}$  (FE) the full width at half maximum.

### 3.3. Intensity stability of the photoluminescence spectra

The influence of the LTPL measurement-system-specific parameters on the measurement results is investigated next. Results in **Figure 4a** are based on our CZ reference sample ( $c_B = 1.2 \times 10^{15} \text{ cm}^{-3}$ , illuminated for 60 h before the start of the measurement series) measured for each run. After the initial treatment, the samples were not processed between the runs. All samples, including the reference sample, were measured with the same excitation power measurement sequence (100 mW, 500, 1000, 100 mW (2)). The  $B_{TO}(\text{BE})/I_{TO}(\text{FE})$  ratios from consecutive measurement runs are shown in Figure 4a. The previously mentioned data was used to determine the relative error for the LTPL measurements. The relative error is the standard deviation of these  $B_{TO}(\text{BE})/I_{TO}(\text{FE})$  ratios divided by their mean value. The error was determined separately for each excitation power. Figure 4b shows the reference sample in a measurement

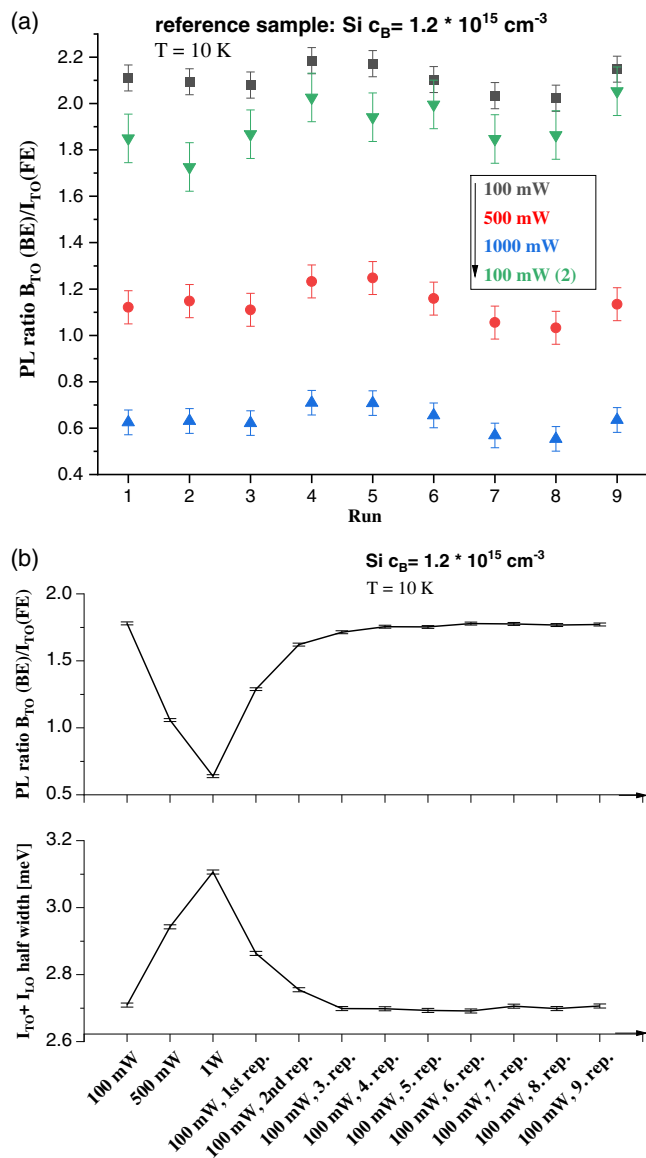


**Figure 4.** a) The PL ratio  $B_{TO}(BE)/I_{TO}(FE)$  over all runs of a reference sample. b) PL ratio and  $I_{TO} + I_{LO}(FE)$  full width at half maximum during repeated measurements at different excitation powers.

sequence of 100, 500, 1000 mW, followed by repeated 100 mW measurements on the reference sample. (In all measurements, additional care was taken to ensure that the heating power was stable and equal). The  $B_{TO}(BE)/I_{TO}(FE)$  ratio as along with the  $I(FE)$  full width at half maximum is shown as a function of the measurement sequence. The relative error was determined from the  $B_{TO}(BE)/I_{TO}(FE)$  ratio of the 100 mW measurements starting from the third repetition. Under stable measurement conditions, the  $B_{TO}(BE)/I_{TO}(FE)$  should not fluctuate. The detected peak ratios measured at the same excitation power and measurement sequence should match. In Figure 4a, the PL ratio varies by up to 8 %. In Figure 4b, with repeated 100 mW excitation power, the peaks remain stable. An error of only 1% is determined starting from the third repeated

**Table 2.** Comparison of the reference sample (see Figure 4a) temperatures determined by fit during the measurement sequence: (100 mW ( $T_1$ ), 500, 1000, 100 mW ( $T_2$ )).

Treatment (I)	$c_B = 1.22 \times 10^{15} \text{ cm}^{-3}$	
RUN	$T_1$ [K]	$T_2$ [K]
1	10.45	10.63
2	10.57	10.92
3	10.61	10.73
4	10.48	10.61
5	10.55	10.74
6	10.55	10.74
7	10.66	10.77
8	10.82	10.96
9	10.53	10.90

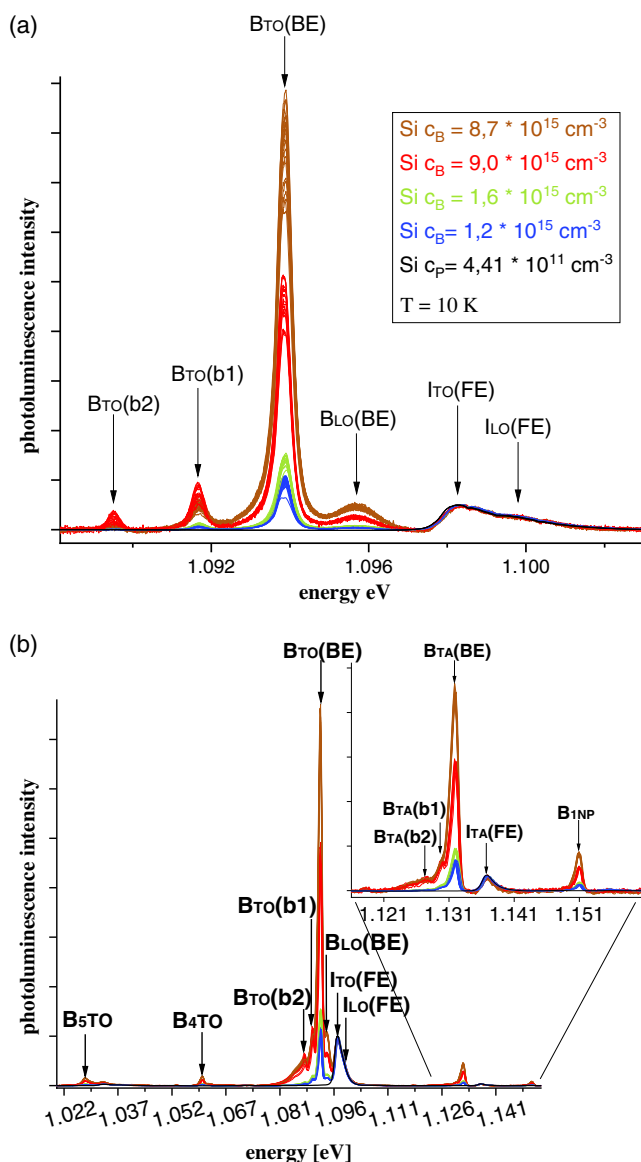
100 mW measurement. The second 100 mW measurements in Figure 4a showed smaller PL intensity ratios. In Figure 4b, the PL ratio of the first 100 mW measurement recovers to its original value after the third repeated 100 mW measurement. At that moment the peak intensity variations within the same excitation power measurement sequence cannot be explained. To explain the reduction in the  $B_{TO}(BE)/I_{TO}(FE)$  ratio between the first and second 100 mW measurement, we consider Table 2. The error bars of all other diagrams are based on the relative error of Figure 4a, since it turns out to be larger than in the test series shown in Figure 4b.

Table 2 lists sample temperatures' results obtained by fitting the  $I_{TO} + I_{LO}(FE)$  PL peak. In all cases, the second 100 mW measurement has a higher temperature. Here the heating of the sample due to the excitation laser can be observed over the measurement sequence (100 mW ( $T_1$ ), 500, 1000, 100 mW ( $T_2$ )). We managed to determine a significant influence of the system parameters of the LTPL spectroscopy on the intensity ratios and the stability of the measured data. It is clear that the excitation heats the sample locally. The helium gas flow in the cryostat is not sufficient to keep the sample temperature constant at 10 K. Thus, a waiting step is a must between measurements. On closer examination, the sample temperature is not the only factor influencing the  $B_{TO}/I_{TO}$  ratio. By comparing Figure 4a and Table 2, it can be seen that the  $B_{TO}/I_{TO}$  ratio is strongly dependent on the sample temperature. However, from Figure 4b, it can be seen that temperature cannot be the only factor influencing the  $B_{TO}/I_{TO}$  instability. For example, the  $B_{TO}/I_{TO}$  ratios are still not the same at very similar temperatures (see Table 2,  $T_1$ , RUN 2,5,6,9). Therefore, we decided against back-calculating the  $B_{TO}/I_{TO}$  ratio in order not to unintentionally falsify the measurement data.

#### 3.4. LID related LTPL peak

To investigate the presence of an additional PL signal related to the LID in boron-doped silicon, we analyzed differently treated samples (five differently doped Si wafers) by LTPL. The graphs in Figure 5 show the PL spectra as a function of photon energy. Four wafers are boron doped and one phosphorus doped. The





**Figure 5.** LTPL spectra of different boron- (B) and phosphorous (P)-doped samples. The spectra are normalized with respect to the height of the free exciton  $I_{TO}(FE)$  peak. The measurement conditions are: 100 mW excitation power and 1200 grooves  $mm^{-1}$  (for a)) and 150 grooves  $mm^{-1}$  (for b)). The different lines (together 95 spectra for (a) and 45 spectra for (b)) of a color contain measurements after different sample treatments (see Figure 6).

data are shown in Table 1. The high-resistance Si sample  $c_P = 4.41 \times 10^{11} cm^{-3}$  was used as a reference sample. The spectra were normalized to the  $I_{TO}(FE)$  peak. The samples of each wafer were prepared based on the experience of LID. Experience shows that degradation of charge carrier lifetime occurs in two steps under illumination (abbreviation: I for the long illumination, i for the short illumination) and can be restored to the initial lifetime by one annealing step (200 °C, 10 min; abbreviation: t). The first degradation under illumination occurs within a few minutes to hours and the second step of degradation from hours to days. The exact treatment is described in the Experimental Section. The LID defect ( $A_{Si}-Si_i$  defect) can be

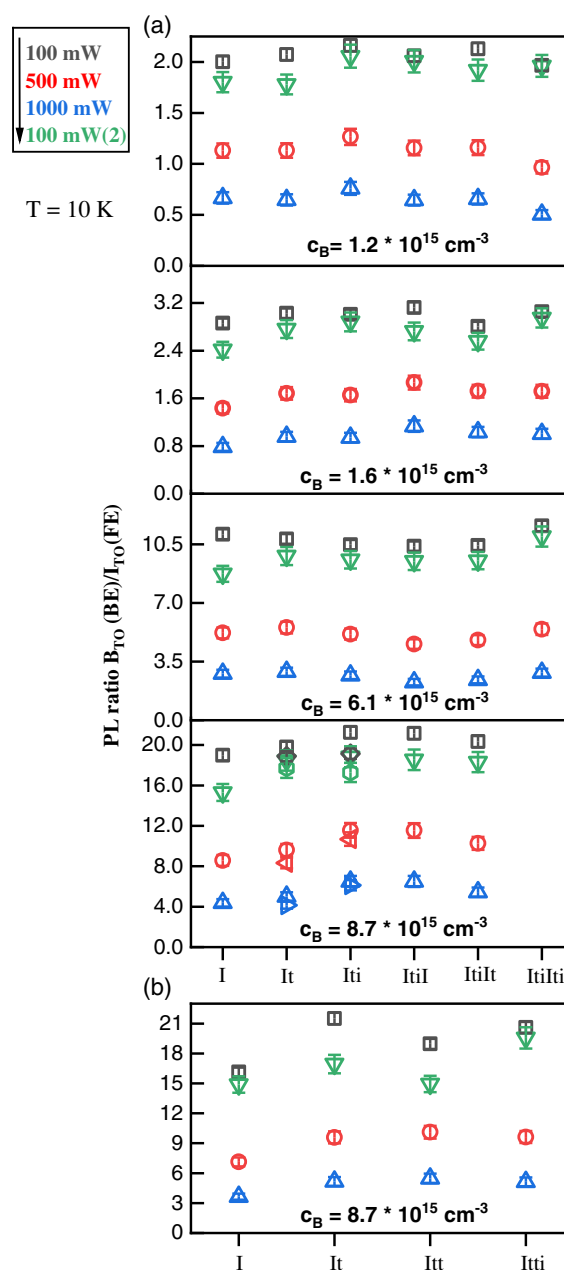


**Figure 6.** a) The PL ratio  $B_{TO}(BE)/I_{TO}(FE)$  during the LID cycle and a b) repeated anneal followed by illumination of boron-doped CZ silicon. Different symbols in the same color represent data from different samples.

in different defect configurations according to Lauer et al.<sup>[19]</sup> These configurations are influenced not only by the current sample treatment (illumination, annealing), but also by the currently present defect state. Therefore, great importance is attached to the exact description of the sample treatment. **Figure 6** shows the sample treatment on the x-axis. The treatment sequence read from left to right. Figure 5a shows the PL spectra detected with the 1200 grooves  $mm^{-1}$  grid. These PL spectra range from 1.088 to 1.101 eV. Figure 5b shows the overview spectra detected with the 150 grooves  $mm^{-1}$  grid. The photon energy ranges from 1.022 to 1.141 eV.

In Figure 5a, we expected the formation of an additional emission line. The emission line should correlate to the activation of the LID defect. According to Vaquero-Contreras et al.<sup>[5]</sup> this additional peak forms as a shoulder of the  $B_{TO}(BE)$  peak. This shoulder was detected after 60 h illumination at one sun.

Defect formation during illumination could cause a reduction in  $B_{TO}(BE)$  intensity. Here, the defect formation leads to a reduction of the luminescent excitonic transitions, according to Broussell et al.<sup>[10]</sup>

Figure 5b is shown to check for the existence of an additional excitonic transition in the TA or NP region. This peak should be analogous to the P line of the  $In_{Si}-Si_i$  defect. Here, the P line forms after about 1 h illumination at 1 sun (slow LID part). After annealing at 200 °C for 10 min, it disappears again, according to Lauer et al.<sup>[8]</sup>

As a first result of these measurements in Figure 5, no  $B_{TO}(BE)$  shoulder is seen in any of the 95 PL spectra. We observe a slight change in the  $B_{TO}(BE)/I_{TO}(FE)$  ratios. Figure 6 shows this in more detail. No equivalent to the P line in indium-doped silicon is seen in Figure 5b in 45 spectra. The normalized  $I_{TO} + I_{LO}(FE)$  peak shows the same line shape for all 95 measurements of all dopants and runs.

In Figure 5a, fluctuations in  $B_{TO}(BE)$  intensity could be detected. For further analysis, Figure 6 compares the peak intensity ratios of samples with different treatments. The correlation between the defect formation and the  $B_{TO}(BE)$  intensity should be analyzed. Figure 6a,b shows the evaluation of the PL spectra with respect to their  $B_{TO}(BE)/I_{TO}(FE)$  ratio. Samples from four differently doped wafers were analyzed. The measurement sequence was (100, 500, 1000, and again 100 mW). The PL intensities are normalized to the  $I_{TO}(FE)$  peak. The sensor temperature was around  $T = 10$  K. In Figure 6a, the sample treatments follow the LID cycle according to Lauer et al. and Bothe and Schmidt.<sup>[5,8]</sup> Figure 6b shows the  $B_{TO}(BE)/I_{TO}(FE)$  ratio with respect to a deviating treatment method. It consists of additional annealing. This process ensures that all defects have been eliminated or are in the ground state. As previously mentioned, the collapse of  $B_{TO}(BE)$  intensity due to defect formation was explained in other publications.<sup>[10]</sup> According to Bothe and Schmidt,<sup>[5]</sup> the generated defects can recover. For this, samples with boron dopants above  $\geq 1 \Omega cm$  are annealed at 200 °C for 10 min.

The measurement shows a significant change in the  $B_{TO}(BE)/I_{TO}(FE)$  ratios. The variation of the peak ratios lies outside the determined error. However, it does not depend on the LID cycle (see Figure 6a). In Figure 6b, no apparent influence on the intensity ratio on the LID cycle can be seen, too. **Figure 7** visualizes the instability of the  $B_{TO}(BE)$  line with respect to its intensity.

The question of why a P line appears in In- and Tl-doped silicon according to Watkins et al.<sup>[20]</sup> but not in our experiments on B-doped silicon is not easily answered. First, it must be mentioned that the P line was not found in In-doped samples used for the LID investigations by carrier lifetime measurements. This is similar to our experiments here where we used as-grown CZ silicon samples for the LTPL studies. The P line was found only in In-implanted samples. This unique line could be a breakthrough point into implanting boron and applying the “P line generation procedure” according to Terashima and Matsuda.<sup>[21]</sup>

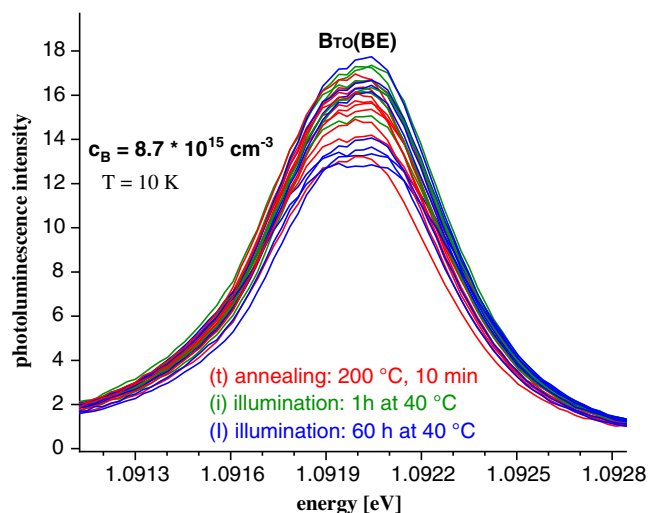


**Figure 7.** LTPL  $B_{TO}(BE)$  line of various treatments (the different colors show the last sample treatment in each case) as a function of photon energy. The excitation power is 100 mW, and the spectra are normalized to  $I_{TO}(FE)$  peak.

to observe a line in boron-doped silicon too. This project will be introduced in the future contributions.

Second, there might be principal differences between the larger  $In_{Si}-Si_i$  and  $Tl_{Si}-Si_i$  defects compared with the small  $B_{Si}-Si_i$  defect. It could be possible that the configuration of the  $As_{Si}-Si_i$  defects in the case of indium and thallium is due to size effects different to the boron case. Hence, it could be possible that the photoelectron or hole cannot bind locally to the defect in the boron case. In consequence, no isoelectronic bound exciton can exist. In the near future, we plan to simulate the configurations of the neutral  $As_{Si}-Si_i$  defect for boron, indium, and thallium.

Figure 7 illustrates the PL  $B_{TO}(BE)$  peak of wafer  $c_B = 8.7 \times 10^{15} cm^{-3}$ . The spectra are normalized to the  $I_{TO}(FE)$  peak. Here the different sample treatments are shown in color. The treatments are described in detail in the Experimental Section. Assuming that the LID defect does not affect  $B_{TO}(BE)$  intensity, a stable peak is expected. If the LID cycle occurs due to silicon–boron pair bonding, an influence of the sample treatment on the  $B_{TO}(BE)$  intensity could be expected. The  $B_{TO}(BE)$  intensity is unstable. However, the sample treatment shows no obvious influence. Therefore, we assume that no  $B_{Si}-Si_i$  pair formation takes place during the LID cycle. An analogous behavior to iron–boron pair formation does not seem to be present. Thus, the  $B_{Si}-Si_i$  defect will not be formed during the LID cycle but is already present in the crystal. This LID defect is activated by illumination.

However, there should be an influence of carrier lifetime on the  $B_{TO}/I_{TO}$  ratio. The excess carrier density is affected by both the excitation power and the carrier lifetime. This influence is probably too small, considering there are many parameters that also influence the  $B_{TO}/I_{TO}$  ratio such as excitation power, sample temperature, and nonradiative recombination processes.<sup>[22]</sup>

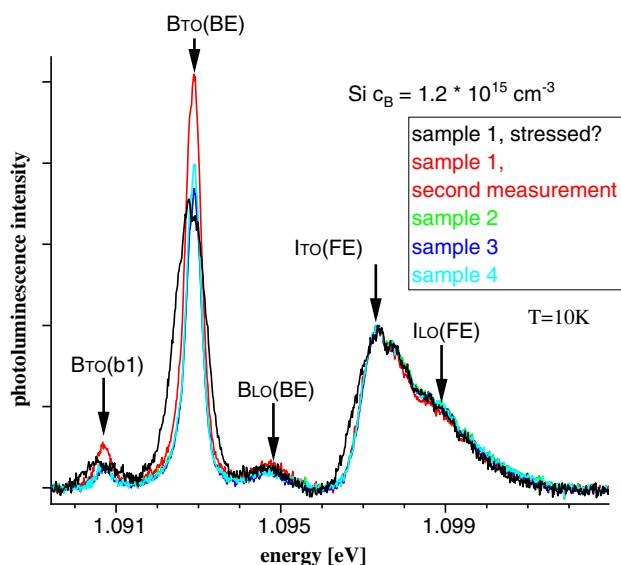


**Figure 8.** LTPL spectra of samples from the same wafer. All samples were illuminated for 24 h at 40 °C and 1 sun.

### 3.5. Peak Shoulder/stressed Samples

It should not remain unmentioned that in our many measurements of samples of different treatments, we once detected a shoulder of the  $B_{TO}(BE)$  peak (black line in **Figure 8**). **Figure 8** compares four samples from the same wafer  $Si\ c_B = 1.2 \times 10^{15}\text{ cm}^{-3}$  with the same treatment (24 h, 1 sun, 40 °C). The measurement depicted as a black line is validated as follows; the sample was removed from the sample holder and measured again in another run (red spectrum) along with three other sample pieces. The excitation power was 100 mW. Please note that the  $B_{TO}(BE)/I_{TO}(FE)$  ratio varies. No attention was paid to the stability of the heating power when recording this test series. The stability of a measurement is shown here in the  $B_{TO}/I_{TO}$  ratio. The heating power influences the helium gas flow and thus the sample temperature. In this case, however, the aim was not to make a reproducible measurement of the  $B_{TO}/I_{TO}$  ratio. The focus was on the presence of a shoulder at the  $B_{TO}$  peak. The sensor temperature was  $T = 10\text{ K}$ .

A shoulder of the  $B_{TO}(BE)$  peak structure was discovered by M. Vaqueiro-Contreras et al. in relation to the LID cycle.<sup>[9]</sup> In our measurements, only sample 1 showed a shoulder at the  $B_{TO}(BE)$  peak. After sample 1 was reinstalled and measured again, the shoulder cannot be detected anymore. All other samples of the same wafer and treatment also show no shoulder in their PL spectra. Here, the shoulder of the  $B_{TO}(BE)$  peak neither appeared in the additional sample measurement nor in any further treatment. We conclude that the double-peak line structure was caused by the moderate stress of the sample due to the screw pressure (this is how the sample was fixed) or by water ice. We show these measurements because we could see the shoulder here uniquely and randomly on the samples of the wafers. In this way, we wanted to show that it is possible for such stresses to occur randomly on the sample and that the shoulder is not caused by the defect. Our assumption is confirmed by the studies

of Karasyuk et al.<sup>[23,24]</sup> The Jahn–Teller effect is observed in the no-phonon (NP) area due to pressure on the sample. The uniaxial stress on the boron-doped Si samples induces a splitting of the bound-excitonic (BE) states. We were also able to reproduce analogous shoulder or double-peak structures by applying targeted mechanical stresses to boron-doped silicon samples, further confirming our assumption.

## 4. Conclusion

Boron-doped CZ silicon is widely used in industry and suffers from LID. We are on the way to understand the structure of the defect in more detail. For this purpose, we investigated the LID defect by performing LTPL measurements. The samples were treated differently and subsequently measured. Treatments followed the LID cycle with illumination for 60 h at 40 °C and one sun intensity, annealing for 10 min at 200 °C in the dark and illumination for 1 h at 40 °C and one sun intensity. The LID cycle was also investigated by MWPCD measurements. A suitable method to determine the sample temperature during the measurement was found and used to draw conclusions about the measurement stability. Four-point-probe measurements were used to determine the dopant concentration. Using these methods, we investigated whether LID dependence on the LTPL spectra in the form of an additional peak or shoulder of the  $B_{TO}(BE)$  peak or a change of the  $B_{TO}(BE)/I_{TO}(FE)$  ratio can be observed. Under illumination, the charge carrier lifetime decreases in two steps shown by our MWPCD measurements. During LTPL measurements, we could not observe any reproducible impact of the LID cycle sample treatments on the spectra. Furthermore, in over 900 measurements, a shoulder at the  $B_{TO}(BE)$  peak was observed only once. This observed shoulder could not be reproduced. The shoulder at the  $B_{TO}(BE)$  peak is possibly caused by stress on the sample. Likewise, no additional PL line could be observed. However, a significant influence of the LTPL's system parameters on the stability of the PL signals was found. **The assumption that the formation of silicon–boron pairs would lead to a decrease in the  $B_{TO}(BE)$  peak intensity could not be confirmed.**

## Acknowledgements

This project was funded by the Deutsche Forschungsgemeinschaft (DFG, German Research Foundation), 44512322, SimASiSii. Younes Slimi (TU Ilmenau, Institute of Physics) is greatly acknowledged for the grammatical review of the paper.

Open Access funding enabled and organized by Projekt DEAL.

## Conflict of Interest

The authors declare no conflict of interest.

## Data Availability Statement

The data that support the findings of this study are openly available in [Supplementary Material: Low temperature photoluminescence investigation of light-induced degradation in boron doped CZ-silicon] at [10.5281/zenodo.6358812], reference number [6358812].



## Keywords

boron-doped Czochralski silicon, crystal defects, four-point-probe measurements, light-induced degradations, low-temperature photoluminescence

Received: March 15, 2022

Revised: July 3, 2022

Published online: July 30, 2022

- [1] R. L. Crabb, in *Proc. of the 9th IEEE Photovoltaic Specialists Conf.*, IEEE, New York **1972**, p. 329.
- [2] H. Fischer, W. Pschunder, in *Proc. of the Tenth IEEE Photovoltaic Specialists Conf.*, IEEE, New York **1973**, p. 404.
- [3] J. Lindroos, H. Savin, *Sol. Energy Mater. Sol. Cells* **2016**, *147*, 115.
- [4] T. Niewelt, J. Schon, W. Warta, S. W. Glunz, M. C. Schubert, *EEE J. Photovoltaics* **2016**, *7*, 1.
- [5] K. Bothe, J. Schmidt, *J. Appl. Phys.* **2006**, *99*, 013701.
- [6] J. Schmidt, *Solid State Phenom.* **2004**, *95–96*, 187.
- [7] K. Lauer, C. Möller, D. Schulze, C. Ahrens, J. Vanhellefont, *Solid State Phenom.* **2015**, *242*, 90.
- [8] K. Lauer, C. Möller, D. Schulze, C. Ahrens, *AIP Adv.* **2015**, *5*, 017101.
- [9] M. Vaqueiro-Contreras, V. P. Markevich, J. Coutinho, P. Santos, I. F. Crowe, M. P. Halsall, I. Hawkins, S. B. Lastovskii, L. I. Murin, A. R. Peaker, *J. Appl. Phys.* **2019**, *125*, 185704.
- [10] I. Broussell, V. A. Karasyuk, M. L. W. Thewalt, *Appl. Phys. Lett.* **2001**, *78*, 3070.
- [11] C. Möller, K. Lauer, *Phys. Status Solidi RRL* **2013**, *7*, 461.
- [12] Semiconductor Equipment and Materials International, SEMI MF1389-0704 **2004**.
- [13] P. J. Dean, J. R. Haynes, W. F. Flood, *Phys. Rev.* **1967**, *161*, 711.
- [14] M. Tajima, *Jpn. J. Appl. Phys.* **1982**, *21S1*, 113.
- [15] K. Lauer, A. Laades, H. Übensee, H. Metzner, A. Lawrenz, *J. Appl. Phys.* **2008**, *104*, 104503.
- [16] I. Pelant, J. DianDian, J. Matouskova, J. Valenta, J. Hala, M. Ambroz, M. Vacha, *J. Appl. Phys.* **1993**, *73*, 3477.
- [17] T. Iwai, M. Tajima, A. Ogura, *Phys. Status Solidi C* **2011**, *8*, 792.
- [18] K. Lauer, C. Möller, D. Schulze, T. Bartel, F. Kirscht, *Phys. Status Solidi RRL* **2013**, *7*, 265.
- [19] K. Lauer, C. Möller, C. Tessmann, D. Schulze, N. V. Abrosimov, *Phys. Status Solidi C* **2017**, *14*, 1600033.
- [20] S. P. Watkins, M. L. W. Thewalt, T. Steiner, *Phys. Rev. B* **1984**, *29*, 5727.
- [21] K. Terashima, T. Matsuda, *Jpn. J. Appl. Phys.* **2002**, *41*, 1203.
- [22] S. Binetti, A. Le Donne, A. Sassella, *Sol. Energy Mater. Sol. Cells* **2014**, *130*, 696.
- [23] V. A. Karasyuk, S. An, M. L. W. Thewalt, E. C. Lightowers, A. S. Kaminskii, *Solid State Commun.* **1995**, *93*, 379.
- [24] V. A. Karasyuk, A. G. Steele, A. Mainwood, E. C. Lightowers, G. Davies, D. M. Brake, M. L. W. Thewalt, *Phys. Rev. B* **1992**, *45*, 11736.